Available online at www.sciencedirect.com
SCIENCE DIRECT®
International Journal of Thermal Sciences 45 (2006) 917–922
International Journal of Thermal Sciences
www.elsevier.com/locate/ijts

Natural convection in a 2D-cavity with vertical isothermal walls: Cross-validation of two numerical solutions

A. Barletta [a,*], E. Nobile [b], F. Pinto [b], E. Rossi di Schio [a], E. Zanchini [a]

[a] *Dipartimento di Ingegneria Energetica, Nucleare e del Controllo Ambientale (DIENCA), Università di Bologna, Viale Risorgimento 2, I-40136 Bologna, Italy*
[b] *Dipartimento di Ingegneria Navale, del Mare e per l'Ambiente (DINMA), Università di Trieste, Via Valerio 10, I-34127 Trieste, Italy*

Received 13 July 2005; received in revised form 2 December 2005; accepted 5 December 2005

Available online 19 January 2006

Abstract

In this paper, a numerical study of natural convection in a 2D-enclosure is presented. The enclosure is bounded by two vertical isothermal walls, kept at different temperatures, and by two adiabatic walls which are either straight and horizontal (rectangular cavity) or elliptic (modified rectangular cavity). The dimensionless mass, momentum and energy balance equations are solved by means of two different software packages based on Galerkin finite element methods. An excellent agreement between the solutions is found and provides a cross-validation of the results. Two basic geometries are considered: a square geometry and a rectangular one with height double the width. For each basic geometry, three cavities are investigated: a rectangular cavity, and two modified rectangular cavities. Dry air is considered, with several values of the Rayleigh number. The results show that the elliptic boundaries enhance the mean Nusselt number and the dimensionless mean kinetic energy of the fluid.

Keywords: Natural convection; Enclosure; Laminar flow; Boussinesq approximation; Numerical methods

1. Introduction

In the literature, the natural convection in 2D rectangular cavities with two isothermal and two adiabatic walls has been widely investigated. Indeed, this convection problem has many technical applications, such as thermal insulation in buildings and solar collector design. Particular attention has been devoted to the case of vertical isothermal walls [1,2]. Interesting reviews of the theoretical studies on this subject have been presented in [2,3].

The shape of a rectangular cavity is determined by the value of the aspect ratio A, given by the height to width ratio. Analytical solutions refer either to "tall enclosures" ($A \gg 1$), or to "shallow enclosures" ($A \ll 1$). The mean Nusselt number for tall enclosures with vertical isothermal walls has been evaluated by Gill [4] and by Bejan [5]. The mean Nusselt number for shallow enclosures has been evaluated in [6–8]. As it has been pointed out by Bejan [3], when the parameter A has values close to 1, analytical or semi-analytical techniques are no longer applicable; in this case, numerical solutions and experimental investigations must be employed.

Many numerical or experimental papers on natural convection in vertical or inclined rectangular cavities are available in the literature [9–17]. An accurate benchmark solution for free convection of air ($Pr = 0.71$) in a square cavity with vertical boundaries kept at different temperatures is presented in [12], with reference to $10^3 < Ra < 10^6$. In [13] an experimental and numerical analysis of free convection of air in a square inclined cavity is presented. The Authors provide an experimental correlation for the mean Nusselt number, in the range $10^4 < Ra < 10^6$, which is in good agreement with the numerical results reported in [12]. Another benchmark solution for natural convection of air in a square cavity, with the same boundary conditions, is reported in [14] for $10^4 < Ra < 10^6$. The comparison with the results reported in [12] reveals excellent agreement, especially for $Ra = 10^4$ and $Ra = 10^5$. Finally, Nonino and Croce [16] have extended the results presented in [12,14] to the case of higher values assumed by Ra, i.e. $10^5 < Ra < 10^8$. Calculations at even higher values of Ra, which lead to time-dependent solutions, have been reported,

* Corresponding author. Tel.: +39 051 6441703; fax: +39 051 6441747.
E-mail address: antonio.barletta@mail.ing.unibo.it (A. Barletta).

1290-0729/$ – see front matter
doi:10.1016/j.ijthermalsci.2005.12.002

Nomenclature

A, B	aspect ratios
D, H	lengths of the rectangle sides
E_{kin}	dimensionless kinetic energy, defined in Eq. (26)
$\overline{E}_{\mathrm{kin}}$	dimensionless mean kinetic energy, defined in Eq. (27)
g	magnitude of the gravitational acceleration
k	thermal conductivity
L	computational parameter
Nu_m	mean Nusselt number, defined in Eq. (24)
Nu'_m	mean Nusselt number, defined in Eq. (25)
P	difference between the pressure and the hydrostatic pressure
$\hat{p}$	pressure
p	dimensionless pressure, defined in Eq. (9)
Pr	Prandtl number
Ra	Rayleigh number, defined in Eq. (9)
S	dimensionless computational domain
T	temperature
T_h, T_c	wall temperatures
T_0	mean value of the temperature
t	dimensionless temperature, defined in Eq. (9)
U	X component of the fluid velocity
u	dimensionless x-velocity
V	Y component of the fluid velocity
v	dimensionless y-velocity
X, Y	rectangular coordinates
x, y	dimensionless coordinates, defined in Eq. (9)

Greek symbols

α	thermal diffusivity
β	volumetric coefficient of thermal expansion
μ	dynamic viscosity
ν	kinematic viscosity
ϱ_0	mass density for $T = T_0$
Φ, Ψ	functions defined in Eq. (14)

among others, by Le Quéré [18] and Nobile [19]. Recently, the effect of modifications of the cavity shape on the heat transfer rate has been investigated in [17].

In the present paper, the natural convection of a Newtonian fluid in a 2D-cavity is studied numerically. The boundary of the cavity is composed of two vertical isothermal walls, kept at different temperatures, and two adiabatic walls. The latter walls are either horizontal straight lines (rectangular cavity) or elliptic arcs (modified rectangular cavity). The shape of a modified rectangular cavity is characterized by the aspect ratio A, defined above, and the aspect ratio B, given by the ratio between the length of the shorter axis and that of the longer axis of the elliptic arc. The local mass, momentum and energy balance equations are written in a dimensionless form suitable for the numerical solution and solved by means of two different software packages, based on Galerkin finite element methods. The software packages employed are FlexPDE 3.0 (© PDESolutions, Inc. [20]) and FEMLAB 3.0 (© Comsol, AB [21]).

With reference to a Prandtl number equal to 0.71, two values of the aspect ratio A, $A = 1$ and $A = 2$, and three values of the aspect ratio B, $B = 0$ (rectangular cavity), $B = 0.2$ and $B = 0.4$ (modified rectangular cavities), are considered. For each pair of values of the aspect ratios, the temperature field, the velocity field and the mean Nusselt number are evaluated for given values of the Rayleigh number. The results obtained by employing the different software packages are compared. For the special case of a square cavity, a comparison with the results available in the literature is performed. For all the cavities considered, the results obtained with the two packages are in excellent agreement, and the comparison with the benchmark results for the square cavity is also very good. Moreover, it is found that the replacement of straight horizontal walls with elliptic arcs significantly affects the flow and temperature fields, thus yielding an increase of the heat transfer rate.

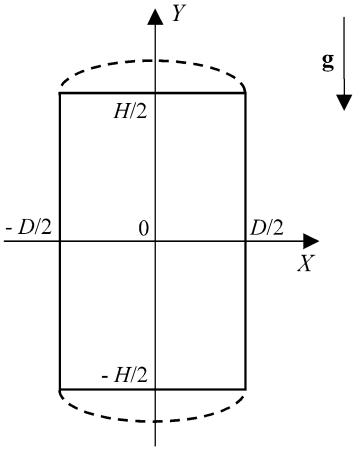

Fig. 1. Drawing of the cavity.

2. Mathematical model

Consider a Newtonian fluid contained in a 2D-cavity bounded by two vertical parallel walls and two walls, which are either straight and parallel (rectangular cavity) or elliptic (modified rectangular cavity), as shown in Fig. 1 together with the chosen coordinate axes (X, Y).

Assuming constant values for the thermal conductivity k, the thermal diffusivity α and the dynamic viscosity μ of the fluid, neglecting the effect of viscous dissipation and adopting the Boussinesq approximation, the mass, momentum and energy balance equations can be written as

$$\frac{\partial U}{\partial X} + \frac{\partial V}{\partial Y} = 0 \tag{1}$$

$$U\frac{\partial U}{\partial X} + V\frac{\partial U}{\partial Y} = -\frac{1}{\varrho_0}\frac{\partial P}{\partial X} + \nu\left(\frac{\partial^2 U}{\partial X^2} + \frac{\partial^2 U}{\partial Y^2}\right) \tag{2}$$

$$U\frac{\partial V}{\partial X}+V\frac{\partial V}{\partial Y} = -\frac{1}{\varrho_0}\frac{\partial P}{\partial Y}+g\beta(T-T_0)+\nu\left(\frac{\partial^2 V}{\partial X^2}+\frac{\partial^2 V}{\partial Y^2}\right) \tag{3}$$

$$U\frac{\partial T}{\partial X}+V\frac{\partial T}{\partial Y}=\alpha\left(\frac{\partial^2 T}{\partial X^2}+\frac{\partial^2 T}{\partial Y^2}\right) \tag{4}$$

In Eqs. (1)–(4), U and V are the velocity components along X and Y, ϱ_0 is the fluid density at the reference temperature T_0, $\nu=\mu/\varrho_0$ is the kinematic viscosity, $\hat{p}$ is the pressure and $P=\hat{p}+\varrho_0 gY$ is the difference between the pressure and the hydrostatic pressure.

The vertical walls are kept isothermal with two different temperatures T_h and T_c, i.e.

$$T\left(-\frac{D}{2},Y\right)=T_h,\qquad T\left(\frac{D}{2},Y\right)=T_c \tag{5}$$

The other walls are adiabatic, i.e. are subjected to the thermal boundary condition

$$\frac{\partial T}{\partial n}=0 \tag{6}$$

where the notation $\partial/\partial n$ indicates the normal derivative.

The reference temperature is chosen as the mean value of the wall temperatures, i.e.

$$T_0=\frac{T_h+T_c}{2} \tag{7}$$

As usual, the boundary conditions for the velocity field are the no-slip conditions, i.e.

$$U=V=0 \tag{8}$$

Let us define the following dimensionless variables:

$$u=\frac{UD}{\alpha},\qquad v=\frac{VD}{\alpha},\qquad t=\frac{T-T_0}{T_h-T_c}$$

$$p=\frac{D^2P}{\varrho_0\alpha\nu},\qquad x=\frac{X}{D},\qquad y=\frac{Y}{D},\qquad A=\frac{H}{D}$$

$$Ra=\frac{g\beta(T_h-T_c)D^3}{\nu\alpha},\qquad Pr=\frac{\nu}{\alpha} \tag{9}$$

On account of Eq. (9), Eqs. (1)–(4) can be rewritten in the dimensionless form

$$\frac{\partial u}{\partial x}+\frac{\partial v}{\partial y}=0 \tag{10}$$

$$\frac{1}{Pr}\left(u\frac{\partial u}{\partial x}+v\frac{\partial u}{\partial y}\right)=-\frac{\partial p}{\partial x}+\frac{\partial^2 u}{\partial x^2}+\frac{\partial^2 u}{\partial y^2} \tag{11}$$

$$\frac{1}{Pr}\left(u\frac{\partial v}{\partial x}+v\frac{\partial v}{\partial y}\right)=-\frac{\partial p}{\partial y}+Ra\,t+\frac{\partial^2 v}{\partial x^2}+\frac{\partial^2 v}{\partial y^2} \tag{12}$$

$$u\frac{\partial t}{\partial x}+v\frac{\partial t}{\partial y}=\frac{\partial^2 t}{\partial x^2}+\frac{\partial^2 t}{\partial y^2} \tag{13}$$

For the use of the software package FlexPDE, Eqs. (10)–(13) must be modified to obtain an equation which contains the Laplacian of the dimensionless pressure p. For this purpose, the following functions are defined:

$$\Phi=u\frac{\partial u}{\partial x}+v\frac{\partial u}{\partial y},\qquad \Psi=u\frac{\partial v}{\partial x}+v\frac{\partial v}{\partial y} \tag{14}$$

On account of Eqs. (10) and (14), by differentiating Eq. (11) with respect to x, Eq. (12) with respect to y, and by summing the obtained equations, one gets:

$$\frac{\partial^2 p}{\partial x^2}+\frac{\partial^2 p}{\partial y^2}=Ra\frac{\partial t}{\partial y}-\frac{1}{Pr}\left(\frac{\partial \Phi}{\partial x}+\frac{\partial \Psi}{\partial y}\right) \tag{15}$$

The set of Eqs. (10)–(13) can be replaced by the set of Eqs. (11)–(13), (15). However, since Eq. (15) has been obtained from the previous set of equations through differentiation, it is not sure that all the solutions of the new set of differential equations satisfy the local mass balance equation, i.e. Eq. (10). For this reason, one can force the validity of Eq. (10) in Eq. (15), by adding to the right-hand side of the latter the left-hand side of Eq. (10) multiplied by an arbitrary parameter L. Thus, the unknown fields u, v, p, and t can be determined by solving either Eqs. (10)–(13) or the following set of differential equations:

$$\frac{\partial^2 p}{\partial x^2}+\frac{\partial^2 p}{\partial y^2} = Ra\frac{\partial t}{\partial y}-\frac{1}{Pr}\left(\frac{\partial \Phi}{\partial x}+\frac{\partial \Psi}{\partial y}\right)+L\left(\frac{\partial u}{\partial x}+\frac{\partial v}{\partial y}\right) \tag{16}$$

$$\frac{\partial^2 u}{\partial x^2}+\frac{\partial^2 u}{\partial y^2}=\frac{\partial p}{\partial x}+\frac{1}{Pr}\Phi \tag{17}$$

$$\frac{\partial^2 v}{\partial x^2}+\frac{\partial^2 v}{\partial y^2}=\frac{\partial p}{\partial y}-Ra\,t+\frac{1}{Pr}\Psi \tag{18}$$

$$\frac{\partial^2 t}{\partial x^2}+\frac{\partial^2 t}{\partial y^2}=u\frac{\partial t}{\partial x}+v\frac{\partial t}{\partial y} \tag{19}$$

The set of differential equations (10)–(13) or (16)–(19) must be coupled with the following boundary conditions:

$$u=v=0\quad\text{on the whole boundary} \tag{20}$$

$$t\left(-\frac{1}{2},y\right)=\frac{1}{2},\qquad t\left(\frac{1}{2},y\right)=-\frac{1}{2} \tag{21}$$

$$\frac{\partial t}{\partial n}=0\quad\text{on the upper and lower walls} \tag{22}$$

It will be assumed that the upper and lower walls have a semi-elliptical shape, with the same eccentricity. As a consequence, the shape of the domain is determined by two dimensionless parameters: the height to width ratio A and the parameter B, which is defined as the ratio between the semi-axes of each ellipsis (Fig. 2). For instance, for $B=0$ the cavity has a rectangular shape, while for $B=1$ the curvilinear walls are semi–circles. Thus, the system of equations (10)–(13) or (16)–(19), coupled with the boundary conditions (20)–(22), determines uniquely the fields u, v, and t for fixed values of the parameters Ra, Pr, A and B. If Eqs. (16)–(19) are used, computations must be performed with increasing values of L, until the dependence of the solution on this parameter becomes negligible.

In Eqs. (10)–(22) only derivatives of the pressure field appear; for this reason, p is determined only up to an arbitrary constant. If FlexPDE is employed, this constant can be fixed, for instance, through the constraint

$$\int_S p\,\mathrm{d}x\,\mathrm{d}y=0 \tag{23}$$

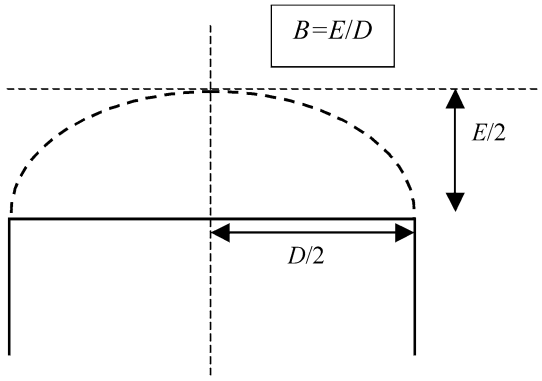

Fig. 2. Drawing of the modified rectangular cavity.

On the other hand, if FEMLAB is employed instead of utilizing Eq. (23) a point value for the dimensionless pressure field is fixed.

The mean Nusselt number can be determined with reference either to the wall $x = -1/2$ or to the wall $x = 1/2$. Thus, one has

$$Nu_m = -\frac{1}{A}\int_{-A/2}^{A/2} \left.\frac{\partial t}{\partial x}\right|_{x\pm 1/2} \mathrm{d}y \tag{24}$$

An energy balance applied to the whole cavity implies that the two mean Nusselt numbers coincide. Another interesting parameter is the dimensionless kinetic energy of the fluid, defined as

$$E_{\mathrm{kin}} = \frac{u^2 + v^2}{2} \tag{25}$$

Obviously, the dimensionless mean kinetic energy of the fluid is given by

$$\overline{E}_{\mathrm{kin}} = \frac{2}{4A + \pi B}\int_S \left(u^2 + v^2\right) \mathrm{d}S \tag{26}$$

3. Numerical solution

The boundary value problem described by Eqs. (16)–(23) has been solved by means of the software package FlexPDE (© PDESolutions, Inc.). FlexPDE creates within the computational domain an unstructured mesh, composed of triangular elements, and refines it iteratively by an adaptive procedure. This procedure ends when a prescribed value of the system-defined accuracy parameter *Errlim* is reached. Additional constraint equations (in our case, Eq. (23)) are allowed. For each set of values of A, B, Ra and Pr, computations have been performed with several different pairs of values of the parameters L and *Errlim*, in order to ensure both the independence of L and the grid independence of the results.

The boundary value problem described by Eqs. (10)–(13) and (20)–(22) has been solved by employing the software package FEMLAB (© Comsol, AB). FEMLAB is a FEM based package to perform equation-based multiphysics modelling. It is possible to perform free-form entry of custom partial differential equations (PDEs) or use specialized physics application modes. A nonlinear solver has been used and the nonlinear tolerance has been set to 1e−11. FEMLAB offers the choice between the use of unstructured triangular meshes and quadrilateral structured ones. Both have been used at different refinement levels. As expected, the structured meshes show to be more efficient in reaching a grid independent result.

In the present paper, the following values of the parameters have been considered: $Pr = 0.71$; $A = 1$ and $A = 2$; $B = 0$, $B = 0.2$ and $B = 0.4$; $Ra = 10^3$, $Ra = 3 \times 10^3$, $Ra = 10^4$, $Ra = 3 \times 10^4$ and $Ra = 10^5$.

4. Results and discussion

First, the square cavity has been investigated, in order to compare the obtained results with the bench-mark solutions available in the literature [10,12]. In Table 1, the values of the mean Nusselt number obtained with FlexPDE and with FEMLAB are compared with those reported in Refs. [10,12], for air ($Pr = 0.71$) and for Ra in the range $10^3 < Ra < 10^5$. The comparison reveals an excellent agreement.

Then, two more geometries have been studied for $A = 1$, having elliptic boundaries with $B = 0.2$ and $B = 0.4$. The obtained values of the mean Nusselt number, reported in Table 2, reveal a good agreement between the results obtained with FlexPDE (Roman) and with FEMLAB (Italic). Moreover, they show that the insertion of the elliptic boundaries strongly enhances the mean Nusselt number, for all the considered values of Ra, even for small values of B. For $B = 0.2$, the increase of Nu_m ranges from 10.5%, for $Ra = 10^5$, to 20.2% for $Ra = 3 \times 10^3$. For $B = 0.4$, the growth of Nu_m ranges from

Table 1
Comparison with the benchmark values of the Nusselt number available in the literature

Ra	Nu_m [12]	Nu_m [14]	Nu_m	
			FlexPDE	Femlab
10^3	1.118	–	1.118	1.118
10^4	2.243	2.245	2.245	2.245
10^5	4.519	4.522	4.520	4.522

Table 2
Mean Nusselt number, for $A = 1$, evaluated with FlexPDE (Roman) or with FEMLAB (*Italic*)

Ra	$B = 0$ Nu_m	$B = 0.2$ Nu_m	$B = 0.4$ Nu_m
10^3	1.118	1.310	1.467
10^3	*1.118*	*1.322*	*1.484*
3×10^3	1.504	1.802	2.010
3×10^3	*1.504*	*1.814*	*2.046*
10^4	2.245	2.614	2.859
10^4	*2.245*	*2.629*	*2.906*
3×10^4	3.141	3.552	3.824
3×10^4	*3.142*	*3.574*	*3.872*
10^5	4.520	4.982	5.268
10^5	*4.522*	*5.007*	*5.308*

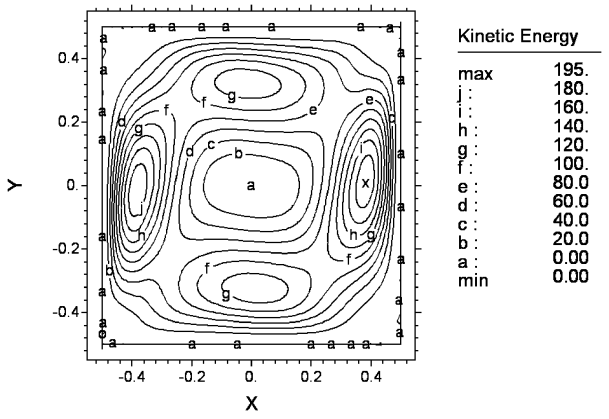

Fig. 3. Contour plots of the dimensionless kinetic energy distribution, for $A = 1$, $B = 0$ and $Ra = 10^4$.

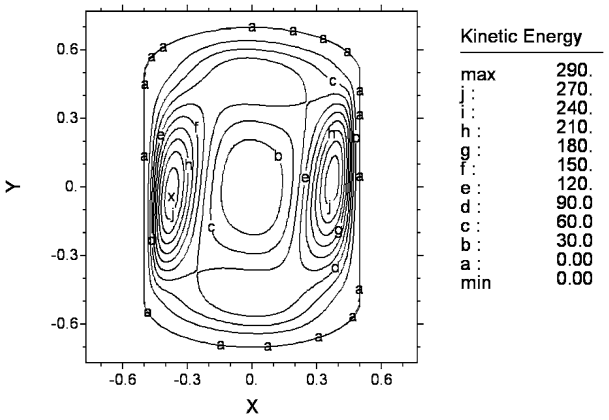

Fig. 4. Contour plots of the dimensionless kinetic energy distribution, for $A = 1$, $B = 0.4$ and $Ra = 10^4$.

17%, for $Ra = 10^5$, to 34.8%, for $Ra = 3 \times 10^3$. The elliptic boundaries enhance the Nusselt number because they assist the convection flow and increase the fluid velocity, especially close to the vertical walls. This effect of the elliptic boundaries is illustrated in Figs. 3 and 4.

Fig. 3 refers to a square cavity with $Ra = 10^4$. It shows that the dimensionless kinetic energy reaches its absolute maximum in two zones close to the isothermal walls, and that two relative maxima take place close to the adiabatic walls. The shape of the cavity forces the flow in circular paths, and determines wide stagnation zones not only in the central core, but also at the corners of the cavity. Fig. 4 refers to a cavity with $A = 1$ and $B = 0.4$, again with $Ra = 10^4$. The figure shows that the elliptic boundaries eliminate the stagnation zones at the corners and enhance the kinetic energy of the fluid close to the vertical walls.

The values of the dimensionless mean kinetic energy of the fluid, for $A = 1$, are reported in Table 3. The table reveals that $E_{\rm kin}$ is both an increasing function of Ra, for each fixed value of B, and an increasing function of B, for each fixed value of Ra. Only for $Ra = 10^5$, the value of $E_{\rm kin}$ decreases if B increases from $B = 0.2$ to $B = 0.4$. However, the local values of $E_{\rm kin}$ close to the isothermal walls increase when B increases from $B = 0.2$ to $B = 0.4$, even for $Ra = 10^5$.

Table 3
Dimensionless mean kinetic energy, for $A = 1$, evaluated with FlexPDE (Roman) or with FEMLAB (*Italic*)

Ra	$B = 0$ $\overline{E}_{\rm kin}$	$B = 0.2$ $\overline{E}_{\rm kin}$	$B = 0.4$ $\overline{E}_{\rm kin}$
10^3	2.920	4.266	5.191
10^3	*2.920*	*4.265*	*5.191*
3×10^3	16.24	21.31	24.33
3×10^3	*16.24*	*21.30*	*24.32*
10^4	64.88	77.72	84.33
10^4	*64.82*	*77.68*	*84.24*
3×10^4	169.6	187.0	191.6
3×10^4	*169.3*	*186.7*	*191.2*
10^5	434.1	449.2	440.0
10^5	*433.2*	*448.5*	*437.4*

Table 4
Mean Nusselt number, for $A = 2$, evaluated with FlexPDE (Roman) or with FEMLAB (*Italic*)

Ra	$B = 0$ Nu_m	$B = 0.2$ Nu_m	$B = 0.4$ Nu_m
10^3	1.191	1.263	1.315
10^3	*1.191*	*1.268*	*1.331*
3×10^3	1.645	1.743	1.813
3×10^3	*1.644*	*1.750*	*1.835*
10^4	2.353	2.486	2.569
10^4	*2.352*	*2.497*	*2.609*
3×10^4	3.147	3.316	3.420
3×10^4	*3.146*	*3.326*	*3.458*
10^5	4.303	4.497	4.606
10^5	*4.301*	*4.508*	*4.648*

Table 5
Dimensionless mean kinetic energy, For $A = 2$, evaluated with FlexPDE (Roman) or with FEMLAB (*Italic*)

Ra	$B = 0$ $\overline{E}_{\rm kin}$	$B = 0.2$ $\overline{E}_{\rm kin}$	$B = 0.4$ $\overline{E}_{\rm kin}$
10^3	8.038	8.606	8.957
10^3	*8.038*	*8.606*	*8.958*
3×10^3	38.99	41.87	43.49
3×10^3	*38.98*	*41.86*	*43.49*
10^4	147.8	158.9	163.9
10^4	*147.6*	*158.6*	*163.6*
3×10^4	368.8	396.6	405.8
3×10^4	*367.4*	*395.1*	*404.1*
10^5	863.6	907.1	907.6
10^5	*857.0*	*899.8*	*900.2*

With reference to the geometries with $A = 2$, the cases $B = 0$ (rectangular cavity), $B = 0.2$ and $B = 0.4$ (modified rectangular cavities) have been investigated. The obtained values of the mean Nusselt number are reported in Table 4, while the values of the dimensionless mean kinetic energy are reported

in Table 5. Again, the results obtained with FlexPDE (Roman) are in good agreement with those obtained through FEMLAB (Italic). Table 4 shows that, with $A = 2$, the insertion of elliptic walls induces an enhancement of the heat exchange smaller than in the case $A = 1$. Similarly, Table 5 shows that the per cent growth of E_{kin} with B is less important for $A = 2$ than for $A = 1$. Finally, a comparison between Tables 3 and 5 reveals that, for any fixed value of Ra, the parameter E_{kin} has higher values for $A = 2$ than for $A = 1$.

5. Conclusions

The natural convection in a 2D-cavity with two vertical isothermal walls, kept at different temperatures, and two adiabatic walls which are either straight (rectangular cavity) or elliptic (modified rectangular cavity), has been investigated. Two numerical software packages, FlexPDE and FEMLAB, have been employed and the results, which refer to dry air, have displayed very good agreement. Values of the Rayleigh number in the range $10^3 \leqslant Ra \leqslant 10^5$ have been considered. The good agreement between the results, together with an excellent agreement with the benchmark solutions for the special case of a square cavity, ensures the reliability of the results obtained. The study has evidenced that, if the straight bottom and top walls of a rectangular cavity are replaced by elliptical walls, a strong enhancement of the mean Nusselt number and of the dimensionless mean kinetic energy of the fluid arises.

References

[1] S. Ostrach, Natural convection in enclosures, Adv. Heat Transfer 8 (1972) 161–227.
[2] B. Gebhart, Y. Jaluria, R.L. Mahajan, B. Sammakia, Buoyancy-Induced Flows and Transport, Hemisphere, New York, 1988, pp. 737–761.
[3] A. Bejan, A synthesis of analytical results for natural convection heat transfer across rectangular enclosures, Int. J. Heat Mass Transfer 23 (1980) 723–726.
[4] A.E. Gill, The boundary layer regime for convection in a rectangular cavity, J. Fluid Mech. 26 (1966) 515–536.
[5] A. Bejan, Note on Gill's solution for free convection in a vertical enclosure, J. Fluid Mech. 90 (1979) 561–568.
[6] D.E. Cormack, L.G. Leal, J. Imberger, Natural convection in a shallow cavity with differentially heated end walls—Part I. Asymptotic theory, J. Fluid Mech. 65 (1974) 209–229.
[7] A. Bejan, C.L. Tien, Laminar natural convection heat transfer in a horizontal cavity with different end temperatures, ASME J. Heat Transfer 100 (1978) 641–647.
[8] G.S. Shiralkar, C.L. Tien, A numerical study of laminar natural convection in shallow cavities, ASME J. Heat Transfer 103 (1981) 226–231.
[9] J.W. Elder, Laminar free convection in a vertical slot, J. Fluid Mech. 23 (1965) 77–98.
[10] M.E. Newell, F.W. Schmidt, Heat transfer by laminar natural convection within rectangular enclosures, ASME J. Heat Transfer 92 (1970) 159–168.
[11] H. Ozoe, H. Sayama, S.W. Churchill, Natural convection in an inclined rectangular channel at various aspect ratios and angles—experimental measurements, Int. J. Heat Mass Transfer 18 (1975) 1425–1431.
[12] G. De Vahl Davis, Natural convection of air in a square cavity: A bench mark numerical solution, Int. J. Numer. Methods Fluids 3 (1983) 249–264.
[13] F.J. Hamadi, J.R. Lloyd, H.Q. Yang, K.T. Yang, Study of local natural convection heat transfer in an inclined enclosure, Int. J. Heat Mass Transfer 32 (1989) 1697–1708.
[14] M. Hortmann, M. Peric', G. Scheuerer, Finite volume multigrid prediction of laminar natural convection: Bench-mark solutions, Int. J. Numer. Methods Fluids 11 (1990) 189–207.
[15] R.A. Kuyper, T.H. Van der Meer, C.J. Hoogendo-orn, R.A.W.M. Henkes, Numerical study of laminar and turbulent natural convection in an inclined square cavity, Int. J. Heat Mass Transfer 36 (1993) 2899–2911.
[16] C. Nonino, G. Croce, An equal-order velocity-pressure algorithm for incompressible thermal flows. Part 2: Validation, Numer. Heat Transfer, Part B: Fund. 32 (1997) 17–35.
[17] L. Adjlout, O. Imine, A. Azzi, M. Belkadi, Laminar natural convection in an inclined cavity with a wavy wall, Int. J. Heat Mass Transfer 45 (2002) 2141–2152.
[18] P. Le Quéré, An improved Chebyshev collocation algorithm for direct simulation of 2D turbulent convection in differentially heated cavities, Finite Element Anal. Design 16 (1994) 271–283.
[19] E. Nobile, Simulation of time-dependent flow in cavities with the additive-correction multigrid method, Part II: Applications, Numer. Heat Transfer Part B 30 (1996) 351–370.
[20] http://www.pdesolutions.com.
[21] http://www.comsol.com.